

Supernova neutrino halo and the suppression of self-induced flavor conversion

Srdjan Sarikas,¹ Irene Tamborra,¹ Georg Raffelt,¹ Lorenz Hüdepohl,² and Hans-Thomas Janka²

¹Max-Planck-Institut für Physik (Werner-Heisenberg-Institut), Föhringer Ring 6, 80805 München, Germany

²Max-Planck-Institut für Astrophysik, Karl-Schwarzschild-Str. 1, 85748 Garching, Germany

(Dated: 4 April 2012, published 19 June 2012)

Neutrinos streaming from a supernova core occasionally scatter in the envelope, producing a small “neutrino halo” with a much broader angle distribution than the primary flux originating directly from the core. Cherry *et al.* have recently pointed out that, during the accretion phase, the halo actually dominates neutrino-neutrino refraction at distances exceeding some 100 km. However, the multiangle matter effect (which increases if the angle distribution is broader) still appears to suppress self-induced flavor conversion during the accretion phase.

PACS numbers: 14.60.Pq, 97.60.Bw

I. INTRODUCTION

Neutrino-neutrino refraction is responsible for the intriguing effect of self-induced flavor conversion [1–5] that can occur in the neutrino flux streaming from a supernova (SN) core [6]. In this context, the angular neutrino distribution plays a crucial role. The current-current structure of low-energy weak interactions implies that the interaction energy between two relativistic particles involves a factor $(1 - \cos \theta)$ where θ is their relative direction of motion.

If the neutrino-emitting region of a supernova core (“neutrino sphere”) has radius R , then at distances $r \gg R$ a typical neutrino-neutrino angle is $\theta \sim R/r$ and $\langle 1 - \cos \theta \rangle \propto (R/r)^2$. The geometric flux dilution provides another factor $(R/r)^2$, leading to an overall $(R/r)^4$ decrease of the neutrino-neutrino interaction energy [6].

In a recent paper, Cherry *et al.* pointed out that this picture is not complete because neutrinos suffer residual collisions on their way out [7]. Every layer of matter above the neutrino sphere is a secondary source, producing a wide-angle “halo” for the forward-peaked primary flux. While the halo flux is small, its broad angular distribution allows it to dominate the neutrino-neutrino interaction energy.

We illustrate the halo with a numerical example, the 280 ms postbounce snapshot of a spherical $15 M_\odot$ model. We recently used it as our benchmark case to study multiangle suppression of self-induced flavor conversion [8]. In Fig. 1 we show the angular dependence of the intensity¹ for the $\bar{\nu}_e$ radiation field, normalized to the forward direction, measured at the radial distances 300, 1000, 3000, and 10,000 km. (The angular distributions become noisy for $\theta \gtrsim \pi/2$, where they are currently not well provided by our simulations.) The core and halo fluxes are two distinct components, the latter so small that it is not visible on a linear plot. If we use $\theta_c \sim 0.1$ as the edge

of the core distribution for the 300 km case, we infer a radius of $R \sim 30$ km for the region where neutrinos begin to stream almost freely. At larger distances, the angular scales are squeezed by a factor R/r .

The impact on neutrino-neutrino refraction is illustrated by the weak potential felt by a radially moving neutrino. In terms of the zenith angle θ of the intensity $\mathcal{I}(\theta)$ we need the quantity

$$\langle 1 - \cos \theta \rangle = \frac{\int_0^\pi d\theta \sin \theta (1 - \cos \theta) \mathcal{I}(\theta)}{\int_0^\pi d\theta \sin \theta \mathcal{I}(\theta)}. \quad (1)$$

For small θ , the integrand in the numerator expands as $(1 - \cos \theta) \sin \theta = \theta^3/2$, allowing the halo to contribute significantly at larger distances where the distributions are more squeezed. At 1000 km, for example, $\langle 1 - \cos \theta \rangle$ is almost a factor of 10 larger than it would be without the halo, in agreement with Cherry *et al.* [7]. The halo parts of the functions in Fig. 1 decrease roughly as θ^{-3} and we find this implies that $\langle 1 - \cos \theta \rangle$ decreases roughly as r^{-1} instead of r^{-2} . The neutrino-neutrino interaction energy then decreases roughly as r^{-3} instead of r^{-4} .

The halo is important during the accretion phase when there is enough matter for the primary flux to scatter on [7]. However, the same high matter density tends to

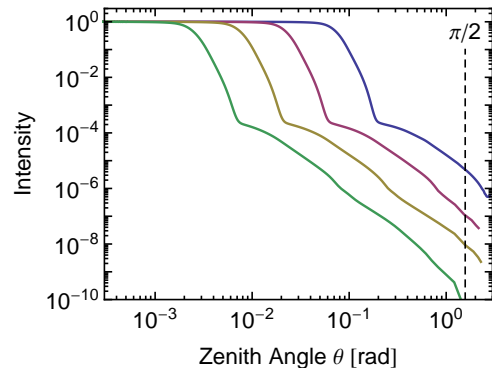


FIG. 1: Intensity for the $\bar{\nu}_e$ radiation field of our numerical model, normalized to the forward direction, measured at the radial distances 300, 1000, 3000, and 10,000 km (right to left).

¹ With “intensity” \mathcal{I} we mean the quantity “neutrinos per unit area per unit time per unit solid angle,” integrated over the energy spectrum.

suppress the self-induced flavor instability [9]. During the early accretion phase, self-induced flavor conversions were found to be typically suppressed [8, 10]. Does the halo change these conclusions? Its importance derives from its broad angle distribution, which also makes it susceptible to the multiangle matter suppression.

To investigate this question, we study in Sec. II the properties of the neutrino halo. In Sec. III we perform a stability analysis along the lines of our recent study of an accretion-phase model [8], and we conclude in Sec. IV.

II. NEUTRINO HALO

A. Numerical angle distribution

Neutrinos stream almost freely and therefore, at larger distances, the angular distributions are simply squeezed to smaller angular scales (Fig. 1). This behavior applies also to the halo flux which, once produced, streams almost freely. At larger distances, the halo distribution primarily gains at the edges: the newly available angular modes get populated by scattering.

The numerical angular distribution at the largest available radius essentially holds all the required information. The decreasing wings of $\mathcal{I}(\theta)$ look like power laws and we can fit the entire distribution by

$$\mathcal{I}_{\text{fit}}(\theta) = \left[\left(\frac{0.9994}{[1 + (\theta/0.0029)^{4.5}]^2} \right)^5 + \left(\frac{0.0006}{[1 + (\theta/0.01)^{1.43}]^2} \right)^5 \right]^{1/5}. \quad (2)$$

We show this function overlaid with the 10^4 km case in Fig. 2. For the other species, the situation is analogous with slightly different parameters.

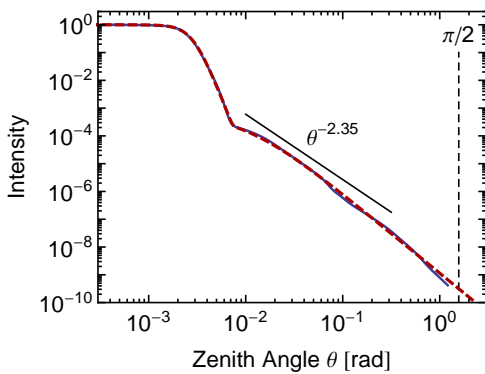


FIG. 2: The 10^4 km numerical case (solid line) overlaid with the analytic fit (dashed line) of Eq. (2). We also indicate the power-law behavior estimated from an analytic argument (Sec. IID).

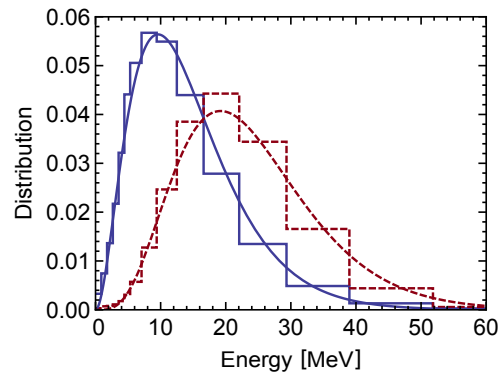


FIG. 3: Energy spectrum of core and halo components. Histogram: Numerical results. Smooth lines: Thermal spectra as described in the text with the same T .

B. Energy distribution

The $\bar{\nu}_e$ flux spectrum emitted from the core roughly follows a thermal Maxwell-Boltzmann form $f_c(E) \propto E^2 e^{-E/T}$. In Fig. 3 we show as a histogram (blue) the numerical spectrum of the core component (measured in the forward direction) together with a thermal fit with $T = 4.8$ MeV (average energy 14.4 MeV).

The halo component arises from scattering on nuclei with a cross section proportional to E^2 . Therefore, the halo spectrum should be $f_h(E) \propto E^4 e^{-E/T}$ with the same T . In Fig. 3 we show as a red histogram the numerical halo spectrum (measured at a very large angle) together with such a fit. In the spirit of an overall consistency check, we find excellent agreement.

C. Neutrino-neutrino refraction

The impact on neutrino-neutrino refraction is quantified by $\langle 1 - \cos \theta \rangle$ as defined in Eq. (1). Motivated by the numerical examples, we first consider truncated power-law intensity distributions of the form

$$\mathcal{I}(\theta) = \begin{cases} 1 & \text{for } \theta \leq \theta_c \\ (\theta_c/\theta)^p & \text{otherwise.} \end{cases} \quad (3)$$

We ask for the asymptotic behavior of $\langle 1 - \cos \theta \rangle$ at large distance, corresponding to $\theta_c \ll 1$. The integrand in Eq. (1) expands as $\sin \theta (1 - \cos \theta) \rightarrow \theta^3/2$. If $p > 4$, the integral is dominated by small angles and we find the result shown in Table I. In other words, if $\mathcal{I}(\theta)$ falls off fast enough, we recover the classic r^{-2} scaling, where we have used that $\theta_c \sim R/r$.

For $p \leq 4$ we can no longer extend the upper integration limit to ∞ and can no longer expand the integrands. With Mathematica we find analytic results with coefficients for $\theta_c \ll 1$ that are given in Table I. In particular, for $p = 3$ the scaling is linear in θ_c .

Next we consider the analytic fit of Eq. (2) and show $\langle 1 - \cos \theta \rangle$ in Fig. 4. We integrate up to $\theta = \pi$ for each ra-

TABLE I: Average $\langle 1 - \cos \theta \rangle$ for $\theta_c \ll 1$ and different p .

Power p	$\langle 1 - \cos \theta \rangle$
∞	$\frac{1}{4} \theta_c^2$
$p > 4$	$\frac{p-2}{p-4} \frac{\theta_c^2}{4}$
4	$(1.1897 - 2 \log \theta_c) \frac{\theta_c^2}{4}$
3	$0.54033 \theta_c$
2	$\frac{1.5788}{1.9929 - 2 \log \theta_c}$
1	0.61712
0	1

dius, which means that we smoothly interpolate between small and large distances. At small radii (inside of the SN core) the distribution is isotropic and $\langle 1 - \cos \theta \rangle = 1$. For $r \lesssim 200$ km we find approximately the naive r^{-2} scaling. At larger distances, the halo becomes important and the scaling turns approximately to r^{-1} . If the halo distribution would scale as θ^{-3} we would expect precisely r^{-1} , but our fit corresponds to $\mathcal{I}(\theta) \propto \theta^{-2.86}$, explaining the less steep variation.

In Fig. 5 we show the enhancement of $\langle 1 - \cos \theta \rangle$ caused by the halo, where we attribute the first part of the analytic fit of Eq. (2) to the core. The enhancement caused by the halo scales almost linearly at large distances. At $r \sim 1000$ km the enhancement is about a factor of 8, roughly in agreement with Cherry *et al.* [7].

D. Analytic halo estimate

For an analytic estimate, we consider a total neutrino production rate $\Phi = L/\langle E \rangle$ emitted from a pointlike source (neutrino luminosity L). It traverses a spherical matter distribution which we model as a decreasing power law of the form $n(r) = n_R(R/r)^m$. We assume that multiple scatterings can be neglected. Every spheri-

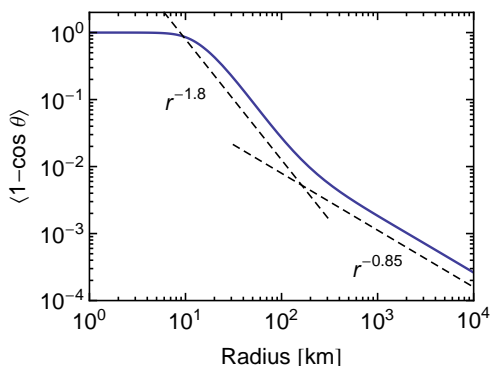
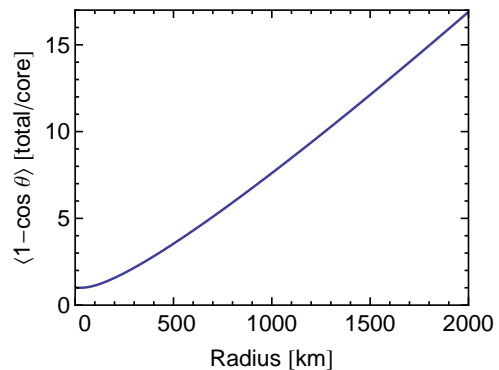
FIG. 4: Average $\langle 1 - \cos \theta \rangle$ for our analytic angle distribution of Eq. (2), representing the 280 ms numerical model.

FIG. 5: Same as Fig. 4, now showing the enhancement caused by the halo, i.e. the ratio total/core contribution, where the core flux is attributed to the first term in Eq. (2).

cal shell is a neutrino source from scattering the primary flux. For the scattering cross section, we assume the form $d\sigma/d\Omega = \sigma_{\text{scatt}}(1 + a \cos \vartheta)/4\pi$, where ϑ is the scattering angle. Elementary geometry (see the Appendix) reveals that at distance r we expect a scattering flux (halo) of

$$\mathcal{I}(r, \theta) = \frac{\Phi \sigma_{\text{scatt}} n_R}{(4\pi)^2 R} \left(\frac{R}{r \sin \theta} \right)^{m+1} \times \int_{\theta}^{\pi} d\vartheta (1 + a \cos \vartheta) \sin^m \vartheta. \quad (4)$$

For small angles, we find a power law $\mathcal{I}(r, \theta) \propto \theta^{-(m+1)}$, whereas the large-angle and backward flux depend on the detailed cross-section angular dependence.

In our numerical example, the density outside the shock wave (at about 70 km) decreases roughly as $r^{-1.35}$ out to about 5000 km. With $m = 1.35$ we expect the halo to vary as $\theta^{-2.35}$ as indicated in Fig. 2. While it would not provide a good global fit, it looks excellent for about the first decade of angles of the halo.

Based on the analytic expression for $\mathcal{I}(r, \theta)$ we can estimate the inward-going flux. It is very small compared to the outward-going core flux, but its contribution to refraction need not be small. We consider a region at sufficiently large radius where neutrino-neutrino refraction is dominated by the halo and ask which fraction is caused by inward-going neutrinos, i.e. which fraction of the integral in Eq. (1) is contributed by $\pi/2 < \theta \leq \pi$. For sufficiently small power-law index m this fraction does not depend on the radius r (to lowest order). Coherent neutrino-nucleus scattering is forward peaked and we use $a = 1$. For $m = 1$ the contribution of the backward flux is 25%, for $m = 2$ approximately 16%.

III. STABILITY ANALYSIS

All previous studies of collective flavor oscillations of SN neutrinos used the free-streaming approximation: it was assumed that collisions play no role in the relevant

stellar region. On the other hand, the halo dominates neutrino-neutrino refraction at larger radii, so in some sense the free-streaming assumption gets worse with distance, not better. Therefore, in order to understand collective flavor conversion in this region, one may have to rethink the overall approach [7].

On the other hand, the multiangle matter effect may still suppress the onset of collective flavor conversions, at least in some accretion-phase models. A linearized stability analysis would still be possible and self-consistent. If self-induced flavor conversions have not occurred up to some radius and if the matter effect is large in that region, then neutrinos continue to be in weak-interaction eigenstates up to small corrections caused by oscillations with the small in-matter effective mixing angle. Therefore, we can use the core+halo flux at that radius as an inner boundary condition for the subsequent evolution. In other words, collisions at smaller radii do not change the conceptual approach, they only provide a broader angular distribution than would have existed otherwise.

A greater problem is how to deal with the inward-going flux which, for our conditions, contributes some 20% to neutrino-neutrino refraction. We will simply neglect it because it cannot be incorporated self-consistently in an approach based on outward-only streaming neutrinos. If the system is stable and stationary, then the picture remains self-consistent because neutrinos remain in flavor eigenstates, including the backward-moving ones.

In this spirit we repeat our linearized flavor stability analysis for our 280 ms snapshot of a $15 M_\odot$ accretion-phase model [8] in a simplified form. We model the angular distribution according to our analytic fit, Eq. (2), which we use at all distances in the form

$$\mathcal{I}(r, \theta) \propto \mathcal{I}_{\text{fit}}(\theta r / 10^4 \text{ km}), \quad (5)$$

because the curves shown in Fig. 1 are almost identical up to an angle scaling. We cut the distribution at $\theta = \pi/2$ to avoid backward-going modes. We assume monoenergetic neutrinos with $\omega_c = \Delta m^2 / 2E_c = 0.5 \text{ km}^{-1}$ for the core flux, i.e. $E_c \sim 12 \text{ MeV}$. We have checked that this choice reproduces well the instability region in Fig. 4 of our previous paper [8] where the full spectrum was used. The halo energies are larger as described in Sec. II B, implying $\langle E_c^{-1} \rangle = 2\langle E_h^{-1} \rangle$, thus we use monoenergetic halo neutrinos with $\omega_h = 0.25 \text{ km}^{-1}$.

The system is unstable in flavor space if the linearized equation of motion discussed in Ref. [8] has eigenvalues with imaginary part κ , the radial growth rate (in units of km^{-1}) of the unstable mode. Whether this growth rate is large or small depends on the available distance. In other words, at a given distance r , the instability is important if $\kappa r \gg 1$ and unimportant if $\kappa r \ll 1$. Therefore, in Fig. 6 we show contours of constant κr in a two-dimensional parameter space consisting of radius r of our model and an assumed electron density n_e which causes the multiangle matter effect.

If we use the core flux alone, this figure contains the same information as Fig. 4 in our previous paper [8]. In

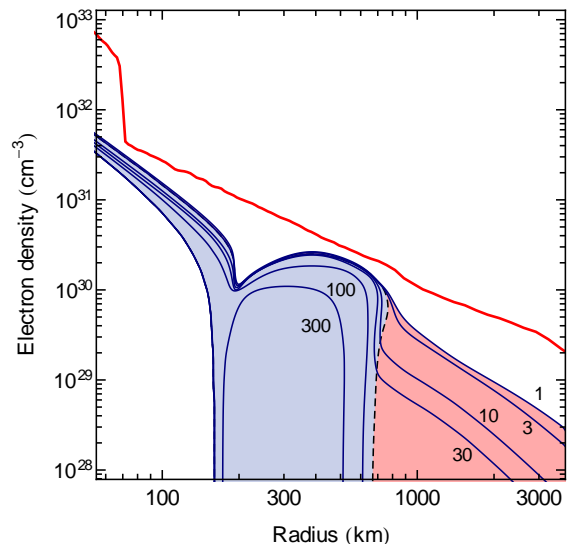


FIG. 6: Contours for the indicated κr values in the parameter space of radius r and assumed electron density n_e . We use a simplified energy spectrum as described in the text. The core flux alone is responsible for $\kappa r \gg 1$ for $r \lesssim 700 \text{ km}$ (blue shading), the halo adds the red-shaded region at larger r . We also show the density profile of our 280 ms numerical model.

the absence of matter, the instability would set in at about 150 km, whereas the presence of matter suppresses the instability entirely: the SN density profile never overlaps with the instability region. The most dangerous region of closest approach is at around 600 km.

In Fig. 6 one clearly sees how the halo flux extends the instability region to larger radii (red shading), but only far away from the SN density profile. In other words, the multiangle matter effect strongly suppresses the would-be instability caused by the halo.

This finding does not contradict the importance of the halo flux for neutrino-neutrino refraction. It is true that the neutrino-neutrino interaction energy caused by the halo was found to decrease roughly as r^{-3} , instead of r^{-4} by the core flux alone. However, the multiangle matter effect is enhanced in a similar way because it depends on the same neutrino angular distribution. A more appropriate comparison is between the neutrino and electron densities. The former decreases as r^{-2} whereas in our model the latter decreases roughly as $r^{-1.35}$ and thus becomes relatively more important with distance. Therefore, it is no surprise that the multiangle matter effect would be more important with increasing distance.

IV. CONCLUSIONS

The halo distribution of neutrinos causes neutrino-neutrino refraction to decrease more slowly with distance than had been thought, but still faster than the matter density during the accretion phase. Repeating our linearized stability analysis including the halo, the system

remains stable for the chosen example. As anticipated, the multiangle matter effect is a crucial ingredient for collective flavor conversions especially in those regions where the halo flux is important.

Thus it remains possible that self-induced flavor conversions are generically suppressed during the early accretion phase. The early signal rise would then encode a measurable imprint of the neutrino mass hierarchy [11].

However, more systematic studies are required to understand if such conclusions are generic. For example, we have assumed that the relatively small backward flux can be neglected for the stability analysis, but its possible role needs to be better understood. Likewise, the role of multi-D effects in SN modeling remains to be explored.

The topic of collective flavor oscillations of SN neutrinos remains a fiendishly complicated problem.

Acknowledgements

This work was partly supported by the Deutsche Forschungsgemeinschaft under Grants No. TR-7 and No. EXC-153, and by the European Union FP7 ITN INVISIBLES (Marie Curie Actions, PITN-GA-2011-289442). I.T. thanks the Alexander von Humboldt Foundation for support.

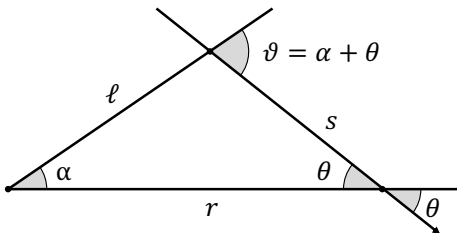


FIG. 7: Geometric definitions for the analytic halo estimate.

Appendix: Analytic Halo Estimate

In order to derive the analytic halo estimate of Eq. (4) we consider a radial distribution of scattering targets, $n(\ell)$, and a differential scattering cross section $d\sigma/d\Omega$. The scattering rate per volume and per solid angle for neutrinos with number density $n_\nu(\ell)$ at radius ℓ is

$$\frac{dq_{\text{scatt}}}{d\Omega} = n_\nu(\ell) n(\ell) c \frac{d\sigma}{d\Omega}, \quad (\text{A.1})$$

where we have reinstated the speed of light. The ‘‘number intensity’’ $\mathcal{I}(r, \theta)$ at radius r of neutrinos scattered to angle direction θ relative to the radius vector at r can be obtained by adding up all scattering contributions along the path s as shown in Fig. 7. It depends on the total neutrino emission rate $\Phi = L/\langle E \rangle$ of the pointlike source assumed to be located at $r = \ell = 0$, which determines the neutrino number density $n_\nu(\ell) = \Phi/(4\pi\ell^2c)$. With this result and Eq. (A.1) one finds

$$\begin{aligned} \mathcal{I}(r, \theta) &= \int_0^\infty ds \frac{dq_{\text{scatt}}}{d\Omega}(\alpha + \theta) \\ &= \int_0^\infty ds \frac{\Phi}{4\pi\ell^2} n(\ell) \frac{d\sigma}{d\Omega}(\alpha + \theta), \end{aligned} \quad (\text{A.2})$$

where $\vartheta = \alpha + \theta$ is the scattering angle and $\ell = r \sin \theta / \sin \vartheta$ and $s = r \sin \alpha / \sin \vartheta$, see Fig. 7.

Using a decreasing power-law distribution of the target density, $n(\ell) = n_R(R/\ell)^m$ with $m \geq 0$, an assumed dependence of the scattering cross section on the scattering angle ϑ of the form $d\sigma(\vartheta)/d\Omega = \sigma_{\text{scatt}}(1 + a \cos \vartheta)/4\pi$, one can transform the integral of Eq. (A.2) into the form of Eq. (4).

-
- [1] S. Samuel, Phys. Rev. D **48**, 1462 (1993); Phys. Rev. D **53**, 5382 (1996). V. A. Kostelecký and S. Samuel, Phys. Lett. B **318**, 127 (1993); Phys. Rev. D **52**, 621 (1995).
 - [2] H. Duan, G. M. Fuller and Y.-Z. Qian, Phys. Rev. D **74**, 123004 (2006). H. Duan, G. M. Fuller, J. Carlson and Y.-Z. Qian, Phys. Rev. D **74**, 105014 (2006).
 - [3] S. Hannestad, G. Raffelt, G. Sigl and Y. Y. Y. Wong, Phys. Rev. D **74**, 105010 (2006); Phys. Rev. D **76**, 029901 (2007). H. Duan, G. M. Fuller, J. Carlson and Y.-Z. Qian, Phys. Rev. D **75**, 125005 (2007).
 - [4] G. G. Raffelt, Phys. Rev. D **83**, 105022 (2011).
 - [5] A. Banerjee, A. Dighe and G. Raffelt, Phys. Rev. D **84**, 053013 (2011).
 - [6] H. Duan, G. M. Fuller and Y.-Z. Qian, Annu. Rev. Nucl. Part. Sci. **60**, 569 (2010).
 - [7] J. F. Cherry, J. Carlson, A. Friedland, G. M. Fuller and A. Vlasenko, arXiv:1203.1607.
 - [8] S. Sarikas, G. G. Raffelt, L. Hüdepohl and H.-T. Janka, Phys. Rev. Lett. **108**, 061101 (2012).
 - [9] A. Esteban-Pretel, A. Mirizzi, S. Pastor, R. Tomàs, G. G. Raffelt, P. D. Serpico and G. Sigl, Phys. Rev. D **78**, 085012 (2008).
 - [10] S. Chakraborty, T. Fischer, A. Mirizzi, N. Saviano and R. Tomàs, Phys. Rev. D **84**, 025002 (2011); Phys. Rev. Lett. **107**, 151101 (2011). N. Saviano, S. Chakraborty, T. Fischer and A. Mirizzi, arXiv:1203.1484.
 - [11] P. D. Serpico, S. Chakraborty, T. Fischer, L. Hüdepohl, H.-T. Janka and A. Mirizzi, Phys. Rev. D **85**, 085031 (2012).